

Wireless Communication with Flexible Reflector: Joint Placement and Rotation Optimization for Coverage Enhancement

Haiquan Lu, Zhi Yu, Yong Zeng, *Senior Member, IEEE*, Shaoan Ma, *Senior Member, IEEE*, Shi Jin, *Fellow, IEEE*, and Rui Zhang, *Fellow, IEEE*

Abstract—Passive metal reflectors for communication enhancement have appealing advantages such as ultra low cost, zero energy expenditure, maintenance-free operation, long life span, and full compatibility with legacy wireless systems. To unleash the full potential of passive reflectors for wireless communications, this paper proposes a new passive reflector architecture, termed *flexible reflector* (FR), for enabling the flexible adjustment of beamforming direction via the FR placement and rotation optimization. We consider the multi-FR aided area coverage enhancement and aim to maximize the minimum expected receive power over all locations within the target coverage area, by jointly optimizing the placement positions and rotation angles of multiple FRs. To gain useful insights, the special case of movable reflector (MR) with fixed rotation is first studied to maximize the expected receive power at a target location, where the optimal single-MR placement positions for electrically large and small reflectors are derived in closed-form, respectively. It is shown that the reflector should be placed at the specular reflection point for electrically large reflector. While for area coverage enhancement, the optimal placement is obtained for the single-MR case and a sequential placement algorithm is proposed for the multi-MR case. Moreover, for the general case of FR, joint placement and rotation design is considered for the single-/multi-FR aided coverage enhancement, respectively. Numerical results are presented which demonstrate significant performance gains of FRs over various benchmark schemes under different practical setups in terms of receive power enhancement.

Index Terms—Flexible reflector (FR), passive reflection, coverage enhancement, joint placement and rotation design.

I. INTRODUCTION

The evolution of mobile communication networks has witnessed the tremendous success of multi-antenna technology,

This work was supported in part by the Natural Science Foundation for Distinguished Young Scholars of Jiangsu Province under Grant BK20240070, in part by the National Natural Science Foundation of China under Grant 62071114, and in part by the Fundamental Research Funds for the Central Universities under Grant 2242022k60004. (*Corresponding author: Yong Zeng.*)

Haiquan Lu, Zhi Yu, Yong Zeng, and Shi Jin are with the National Mobile Communications Research Laboratory and Frontiers Science Center for Mobile Information Communication and Security, Southeast University, Nanjing 210096, China. Haiquan Lu and Yong Zeng are also with the Purple Mountain Laboratories, Nanjing 211111, China (e-mail: haiq_lu@163.com, {zhiyu, yong_zeng, jinshi}@seu.edu.cn).

Shaoan Ma is with the State Key Laboratory of Internet of Things for Smart City and the Department of Electrical and Computer Engineering, University of Macau, Macao SAR, China (e-mail: shaodanma@um.edu.mo).

Rui Zhang is with School of Science and Engineering, Shenzhen Research Institute of Big Data, The Chinese University of Hong Kong, Shenzhen, Guangdong 518172, China (e-mail: rzhang@cuhk.edu.cn). He is also with the Department of Electrical and Computer Engineering, National University of Singapore, Singapore 117583 (e-mail: elezhang@nus.edu.sg).

such as multiple-input multiple-out (MIMO) widely used in the fourth-generation (4G) wireless networks and massive MIMO in the fifth-generation (5G) wireless networks, due to their substantial spatial diversity and multiplexing gains. For the forthcoming sixth-generation (6G) era, massive MIMO is expected to evolve towards extremely large-scale MIMO (XL-MIMO) via scaling up the antenna number by an order of magnitude [1]–[3], e.g., hundreds or even thousands of antennas at the base station (BS), so as to support the ambitious capabilities required by 6G [4]. Despite achieving the unprecedented improvement in the spatial resolution and spectral efficiency, XL-MIMO also faces practical challenges such as expensive hardware cost and high energy expenditure [1], [5]. To address such issues, there has been an upsurge of interest in exploiting various sparse array architectures, including uniform sparse array [6]–[8] and non-uniform sparse array, such as modular, nested, and co-prime arrays [9]–[11]. Compared to the conventional compact array with neighboring elements separated by half wavelength, sparse arrays can achieve a larger array aperture by configuring the antenna spacing larger than half wavelength, without increasing the number of antenna elements. This thus provides improved spatial resolution and degree-of-freedom (DoF) for enhancing both communication and sensing performances.

Besides sparse array, there was extensive research on various cost-effective and energy-efficient hardware architectures for MIMO, such as analog beamforming, lens antenna array, and low-resolution analog-to-digital converter (ADC) [12]. More recently, another promising approach, namely intelligent reflecting surface (IRS) or reconfigurable intelligent surface (RIS) aided communication has been proposed [13]–[16]. Specifically, without any active radio-frequency (RF) chains, IRS is a metasurface consisting of a large number of passive reflecting elements, which are capable of configuring the wireless propagation environment proactively via adjusting their amplitude and/or phase shifts. However, the cost of IRS/RIS increases significantly with its size or number of reflecting elements, especially for that operating at higher frequency bands, which is still practically formidable for large-scale deployment of IRS/RIS in wireless networks.

To further reduce the hardware cost and energy expenditure, fully passive metal reflectors, usually made of copper, aluminum or conductive coating, were also introduced and have gained increasing interest. Initially, the passive reflector was proposed as an alternative of active satellite relays, due

to its simpler operation and maintenance [17], [18]. In the field of antenna design, different types of passive reflectors, such as plane, corner and parabolic reflectors, were utilized to fabricate the reflector antenna, which has been widely applied to the radio astronomy, satellite tracking, and remote sensing [19], [20]. Recently, passive metal reflectors were introduced in wireless communications, aiming at signal/coverage enhancement, channel rank/diversity improvement, interference rejection, secure transmission, and so on. For example, to compensate for the severe penetration loss suffered by millimeter wave (mmWave) communications, passive metal reflectors were deployed to enhance the signal coverage in both indoor [21]–[24] and outdoor scenarios [24], [25]. Moreover, from the perspective of network planning, the deployment of passive reflectors helps to reduce the number of BSs required for area coverage, by jointly designing the placement positions of BSs and passive reflectors [26]. This thus significantly reduces the deployment cost and energy expenditure, as compared to conventional approaches such as increasing transmit power, the number of BSs, access points (APs), relays, and/or antennas [24]. Another appealing benefit for deploying passive reflectors is the MIMO channel rank/diversity improvement, thanks to the creation of additional strong multi-path components [26]–[28]. On the other hand, instead of facilitating the connectivity between desired nodes, passive reflectors can also be deployed to physically block the interference from undesired nodes [29]. Besides, customized wireless communication environment for enhanced security and privacy can be achieved by placing the reflector to block the channel from the legitimate transmitter to malicious users [22], [23].

Note that compared to active BSs/APs or semi-passive IRSs, fully passive metal reflectors possess promising advantages such as ultra low cost, zero energy expenditure, maintenance-free operation and long life span [26], [28]. Moreover, passive reflector is of high compatibility and efficient scalability, which can be integrated into existing and future wireless networks transparently, without changing the network protocol. It is also worth mentioning that the reflection wave of the metal reflector exhibits a beam shape [20], [30], and many efforts have been devoted to mathematically modeling the signal reflection by passive metal reflectors. Specifically, by fixing its normal vector, the scattered field expression of a metal surface was derived in [30]. Furthermore, by taking into account the factors of metal reflector size, orientation and polarization, a more general reflection model was derived in closed-form, followed by experiment measurements to verify its accuracy [28]. Nevertheless, unlike BSs and IRSs, the fully passive architecture renders metal reflectors unable to flexibly adjust the reflection beamforming direction.

The aforementioned works mainly deploy the passive metal reflectors with fixed placement and orientation. This implies that once the metal reflector is deployed, the signal scattered field is determined. Thus, anomalous reflection to any desired direction cannot be achieved in general, unlike the case of IRS. To fully unleash the potential of passive reflector, in this paper, we propose a new architecture for it, termed *flexible reflector* (FR), where the placement position and rotation angle of metal reflector can be flexibly adjusted to dynamically

alter its beamforming direction. In contrast to multi-antenna beamforming which is achieved by dynamically controlling the signal phase of each antenna element, or IRS reflective beamforming by controlling the phase shift of each reflecting element, FR adjusts the placement position and/or rotation angle to manipulate the specular direction, i.e., the beamforming direction. This thus enables a new paradigm of passive beamforming, without relying on RF chains, phase shifters or reflecting elements, nor complex signal processing. Moreover, the practical implementation of FR resembles existing movable antennas (MAs) with position adjustment [31]–[33] as well as six-dimensional movable antennas (6DMAs) with both position and rotation adjustment [34]–[36]. Specifically, by mounting the metal reflector on the motor driven gimbal that can move along a sliding track, the placement and rotation can be adjusted by controlling the electric motors [37]. In this paper, we consider a general multi-FR aided wireless communication system, where one-dimensional (1D) movement and rotation of FR are considered to maximize the minimum expected received signal power across all locations in a given target area. The main contributions of this paper are summarized as follows:

- Firstly, we introduce a multi-FR aided wireless communication system, where a flexible adjustment of passive reflective beamforming direction is enabled by optimizing the placement position and rotation angle of each FR. By deriving the received signal power at any location in terms of each FR's placement and rotation angle, we formulate an optimization problem to maximize the minimum expected receive power across all locations in a given area, subject to the practical placement constraint to avoid overlap and signal blockage, as well as the rotation constraint to ensure the effective reflection.
- Secondly, to gain useful insights, we consider the special case of movable reflector (MR) without rotation. For the special scenario of single-MR aided single target location power enhancement, the optimal MR placement position is derived in closed-form for electrically large or small reflector, respectively. It is analytically shown that the MR should be placed at the specular reflection point for electrically large reflector, and passive beamforming direction adjustment is enabled via placement position optimization. Then, for the scenario of multi-MR aided single target location power enhancement, the placement positions of multiple MRs are jointly designed such that the receiver is located within their beamforming main lobes. Moreover, for area coverage enhancement with a single-MR, the minimum array factor across all locations is derived in closed-form, and its optimal placement is obtained accordingly. Subsequently, a sequential placement algorithm is proposed for the multi-MR case.
- Thirdly, we consider the general case of FR with both placement position and rotation angle adjustments. Starting from the single-FR aided single target location power enhancement, we derive the optimal rotation

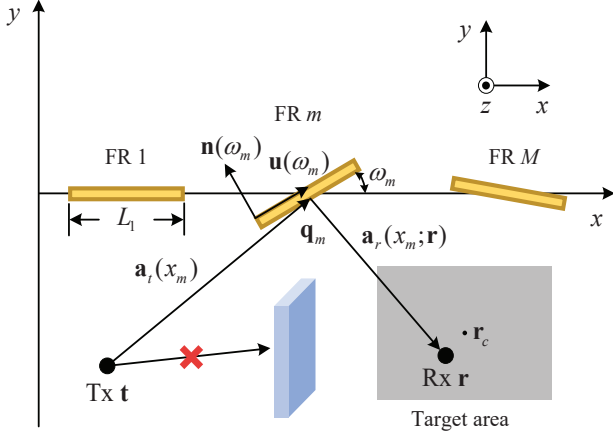


Fig. 1. Wireless communication enhanced by multiple FRs.

angle for the FR with its placement position fixed in closed-form. Then, for the case of multi-FR, the minimum distance between any two FRs to avoid overlap and signal blockage is derived. Next, the joint placement and rotation design is proposed for the single-/multi-FR aided area coverage enhancement scenarios. Finally, extensive numerical results are presented to demonstrate the significant performance gains of FRs over various benchmark schemes under different practical setups.

The rest of this paper is organized as follows. Section II introduces the system model and formulates the optimization problem to maximize the minimum expected receive power across all locations in a given target area. Section III studies the special case of the single-/multi-MR aided coverage enhancement. In Section IV, joint placement and rotation design is considered for the single-/multi-FR aided coverage enhancement by extending MR to FR. Section V provides the numerical results and relevant discussions, and this paper is concluded in Section VI.

Notations: Scalars are denoted by italic letters. Vectors and matrices are denoted by bold-face lower- and upper-case letters, respectively. $\mathbb{C}^{M \times N}$ represents the space of $M \times N$ complex-valued matrices. For a vector \mathbf{x} , $\|\mathbf{x}\|$ denotes its Euclidean norm, and \mathbf{x}^T denotes its transpose. The symbol j denotes the imaginary unit of complex numbers, with $j^2 = -1$. For real number x , $\lfloor x \rfloor$ and $\lceil x \rceil$ denote the floor and ceiling operations, respectively. $\mathbb{E}(\cdot)$ denotes the statistical expectation.

II. SYSTEM MODEL AND PROBLEM FORMULATION

As shown in Fig. 1, we consider a multi-metal plate reflector aided wireless communication system, where M FRs are deployed to assist in the communication from the transmitter (Tx) to the receiver (Rx) at arbitrary location in a given target area \mathcal{A} . The direct link from the Tx to the target area is assumed to be negligible due to blockage. Each reflector is assumed to have size $L_1 \times L_2$, and is centered at the x -axis. The location of the Tx is $\mathbf{t} = [x_t, y_t, 0]^T$. The target area \mathcal{A} is assumed to be a rectangular area on the x - y plane,

and its center is denoted as $\mathbf{r}_c = [x_c, y_c, 0]^T$. The length and width of \mathcal{A} are D_x and D_y , respectively. Thus, any location within \mathcal{A} can be denoted as $\mathbf{r} = [x_r, y_r, 0]^T$, with $x_r \in [x_c - D_x/2, x_c + D_x/2]$ and $y_r \in [y_c - D_y/2, y_c + D_y/2]$. Moreover, the center location of reflector m is denoted as $\mathbf{q}_m = [x_m, 0, 0]^T$, $\forall m \in \mathcal{M}$, with $\mathcal{M} \triangleq \{1, \dots, M\}$. Since the reflectors may move along the x -axis, the notation x_m is used to denote the center location of reflector m . The distance between the Tx and the center of reflector m is $d_t(x_m) = \|\mathbf{q}_m - \mathbf{t}\|$, and that between the center of reflector m and any location \mathbf{r} in \mathcal{A} is $d_r(x_m; \mathbf{r}) = \|\mathbf{r} - \mathbf{q}_m\|$.

Let ω_m denote the 1D rotation angle of reflector m , and the rotation matrix is given by [34], [38]

$$\mathbf{R}(\omega_m) = \begin{bmatrix} \cos \omega_m & -\sin \omega_m & 0 \\ \sin \omega_m & \cos \omega_m & 0 \\ 0 & 0 & 1 \end{bmatrix}. \quad (1)$$

Denote by $\mathbf{u}(\omega_m)$ the normalized direction vector along the edge of reflector m under given rotation angle ω_m , and $\mathbf{n}(\omega_m)$ the corresponding normal direction vector, as illustrated in Fig. 1. Thus, we have

$$\mathbf{u}(\omega_m) = \mathbf{R}(\omega_m) \mathbf{e}_x = \begin{bmatrix} \cos \omega_m \\ \sin \omega_m \\ 0 \end{bmatrix}, \quad (2)$$

$$\mathbf{n}(\omega_m) = \mathbf{R}(\omega_m) \mathbf{e}_y = \begin{bmatrix} -\sin \omega_m \\ \cos \omega_m \\ 0 \end{bmatrix}, \quad (3)$$

where $\mathbf{e}_x = [1, 0, 0]^T$ and $\mathbf{e}_y = [0, 1, 0]^T$ denote the unit vectors along the x - and y -axis, respectively. Let $\mathbf{a}_t(x_m)$ denote the normalized incident vector from the Tx to reflector m , and $\mathbf{a}_r(x_m; \mathbf{r})$ denote the normalized reflection vector from reflector m to location \mathbf{r} . Note that to enable the effective reflection, the Tx and Rx must lie on the same side of the reflector. This yields the following constraint,

$$(\mathbf{a}_t^T(x_m) \mathbf{n}(\omega_m)) (\mathbf{a}_r^T(x_m; \mathbf{r}) \mathbf{n}(\omega_m)) < 0. \quad (4)$$

The signals reflected by two or more times by any FR are assumed to be negligible due to the high path loss. The ratio of the receive power $P_r(x_m, \omega_m; \mathbf{r})$ at location \mathbf{r} to the transmit power P_t via reflector m is given by [20]

$$\frac{P_r(x_m, \omega_m; \mathbf{r})}{P_t} = \frac{\sigma(x_m, \omega_m; \mathbf{r}) \lambda^2}{4\pi(4\pi d_t(x_m) d_r(x_m; \mathbf{r}))^2}, \quad (5)$$

where λ denotes the signal wavelength, and $\sigma(x_m, \omega_m; \mathbf{r})$ denotes the radar cross section (RCS) of reflector m observed at location \mathbf{r} , given by [28]

$$\sigma(x_m, \omega_m; \mathbf{r}) = \sigma_{\max} \eta(x_m, \omega_m; \mathbf{r}) \times \text{sinc}^2(\pi \bar{L}_1 \Delta(x_m, \omega_m; \mathbf{r})), \quad (6)$$

where $\sigma_{\max} \triangleq 4\pi L_1^2 L_2^2 / \lambda^2$ denotes the maximum possible RCS value, $\eta(x_m, \omega_m; \mathbf{r})$ is a factor no greater than one, $\bar{L}_1 \triangleq L_1 / \lambda$ denotes the wavelength-normalized length of the reflector, $\Delta(x_m, \omega_m; \mathbf{r}) \triangleq (\mathbf{a}_r(x_m; \mathbf{r}) - \mathbf{a}_t(x_m))^T \mathbf{u}(\omega_m)$ is the projection of the deflection vector $(\mathbf{a}_r(x_m; \mathbf{r}) - \mathbf{a}_t(x_m))$

along the edge of reflector m , and $\text{sinc}(x) \triangleq \sin(x)/x$. Moreover, the expected receive power at a small region centered at location \mathbf{r} is

$$P_r(\mathbf{r}) = \mathbb{E} \left[\left| \sum_{m=1}^M \sqrt{P_r(x_m, \omega_m; \mathbf{r})} e^{j\varphi_m} \right|^2 \right] \\ = \sum_{m=1}^M P_r(x_m, \omega_m; \mathbf{r}) = \frac{P_t \lambda^2}{(4\pi)^3} \sum_{m=1}^M f(x_m, \omega_m; \mathbf{r}), \quad (7)$$

where φ_m denotes the signal phase of the path via reflector m , with φ_m 's being independent and identically distributed, and $f(x_m, \omega_m; \mathbf{r}) \triangleq \frac{\sigma(x_m, \omega_m; \mathbf{r})}{d_t^2(x_m) d_r^2(x_m; \mathbf{r})}$.

We aim to maximize the minimum (worst-case) expected receive power over all locations in a given target area \mathcal{A} , by jointly optimizing the placement positions $\{x_m\}_{m=1}^M$ and rotation angles $\{\omega_m\}_{m=1}^M$ of the M FRs. The optimization problem can be formulated as (by discarding the constant terms)

$$(P1) \quad \max_{\{x_m, \omega_m\}_{m=1}^M} \min_{\mathbf{r} \in \mathcal{A}} \sum_{m=1}^M f(x_m, \omega_m; \mathbf{r}) \\ \text{s.t. } |x_m - x_n| \geq d_{m,n}^{\min}, \quad \forall m, n \in \mathcal{M}, \quad m \neq n, \\ (\mathbf{a}_t^T(x_m) \mathbf{n}(\omega_m)) (\mathbf{a}_r^T(x_m; \mathbf{r}) \mathbf{n}(\omega_m)) < 0, \quad \forall m, \mathbf{r}, \quad (8)$$

where $d_{m,n}^{\min}$ denotes the minimum distance to avoid the overlap and signal blockage between FRs m and n . Problem (P1) is challenging to be directly solved due to the following two reasons. First, the objective function is the minimum power value across a continuous area, which is difficult to be explicitly expressed in terms of the placement positions and rotation angles of FRs. Second, problem (P1) is a non-convex optimization problem, due to the non-concave objective function and non-convex constraints.

III. MOVABLE REFLECTOR

To gain useful insights for solving (P1), we first study the special case of MRs, by considering their fixed rotation angles $\omega_m = 0, \forall m$.

A. Single Target Location Power Enhancement

In this subsection, we consider the special case of single target location power enhancement, where the scenarios of single- and multi-MR are respectively studied.

1) *Single-MR Case*: As illustrated in Fig. 2, a single-MR is deployed to assist in the communication from the Tx to Rx, where the reflector index is omitted for brevity. Besides, the location \mathbf{r} is omitted in the notations for the case of single target location. The distance between the Tx and the center of the reflector is $d_t(x) = \|\mathbf{q} - \mathbf{t}\| = \sqrt{(x - x_t)^2 + y_t^2}$, and that between the center of the reflector and Rx is $d_r(x) = \|\mathbf{r} - \mathbf{q}\| = \sqrt{(x_r - x)^2 + y_r^2}$. The normalized incident and reflection vectors are $\mathbf{a}_t(x) = \frac{\mathbf{q} - \mathbf{t}}{\|\mathbf{q} - \mathbf{t}\|} = \frac{1}{d_t(x)} [x - x_t, -y_t, 0]^T$ and $\mathbf{a}_r(x) = \frac{\mathbf{r} - \mathbf{q}}{\|\mathbf{r} - \mathbf{q}\|} = \frac{1}{d_r(x)} [x_r - x, y_r, 0]^T$, respectively. With the direction vector along the edge of the reflector $\mathbf{u} = [1, 0, 0]^T$, we have $\Delta(x) = (\mathbf{a}_r(x) - \mathbf{a}_t(x))^T \mathbf{u} =$

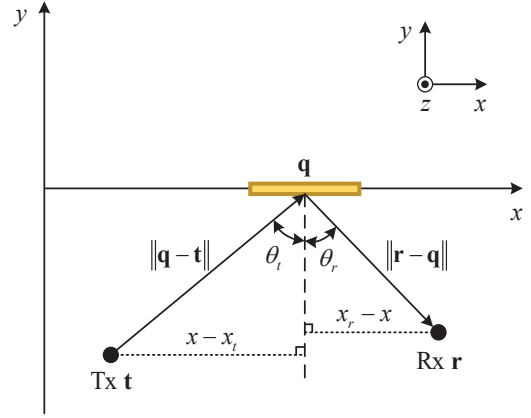


Fig. 2. Single target location power enhancement by a single-MR.

$\frac{x_r - x}{d_r(x)} - \frac{x - x_t}{d_t(x)}$. Besides, the factor $\eta(x)$ is given by $\eta(x) = \frac{y_r^2}{d_r^2(x)}$ [28]. In this case, the function $f(x)$ is expressed as

$$f(x) = \frac{\sigma(x)}{d_t^2(x) d_r^2(x)} = \sigma_{\max} \times \\ \underbrace{\frac{y_r^2}{d_r^2(x) d_r^4(x)}}_{f_1(x)} \underbrace{\text{sinc}^2 \left(\pi \bar{L}_1 \left(\frac{x_r - x}{d_r(x)} - \frac{x - x_t}{d_t(x)} \right) \right)}_{f_2(x)}. \quad (9)$$

Thus, problem (P1) is reduced to

$$\max_x f(x). \quad (10)$$

It is observed from (9) that the function $f(x)$ consists of two terms $f_1(x)$ and $f_2(x)$, where $f_1(x)$ accounts for the factor $\eta(x)$ and the concatenated path loss from the Tx to Rx via the reflector, and $f_2(x)$ can be interpreted as the array factor. Fig. 3 illustrates the values of $f(x)$, $f_1(x)$ and $f_2(x)$ versus the placement position x , by considering $\bar{L}_1 = 10$ and $\bar{L}_1 = 0.1$, respectively. The locations of the Tx and Rx are $\mathbf{t} = [0, -50]^T$ m, and $\mathbf{r} = [100, -150]^T$ m, respectively. It is observed that for electrically large reflector with $\bar{L}_1 = 10$, $f_2(x)$ composed of the sinc function exhibits significant variations as the placement position x changes, as compared to $f_1(x)$. By contrast, for electrically small reflector with $\bar{L}_1 = 0.1$, the impact on $f(x)$ by $f_1(x)$ is more significant than that by $f_2(x)$. This is expected since the sinc function tends to be one when \bar{L}_1 is very small.

Proposition 1: When $\bar{L}_1 \gg 1$, the optimal solution to (10) is

$$x^* = x_t + \frac{y_t}{y_t + y_r} (x_r - x_t). \quad (11)$$

Proof: Please refer to Appendix A. ■

A closer look at Fig. 2 shows that $\sin \theta_t = \frac{x - x_t}{d_t(x)}$ and $\sin \theta_r = \frac{x_r - x}{d_r(x)}$, where θ_t and θ_r denote the incident and reflection angles, respectively. By substituting (11) into $\sin \theta_t$ and $\sin \theta_r$, we have $\sin \theta_t = \sin \theta_r = \frac{x_r - x_t}{\sqrt{(x_r - x_t)^2 + (y_t + y_r)^2}}$.

This implies that for electrically large reflector, the reflector should be placed at the specular reflection point with $\theta_r = \theta_t$.

On the other hand, for electrically small reflector, the placement position variation has a negligible impact on $f_2(x)$, which is expected since the reflector tends to be isotropic. In

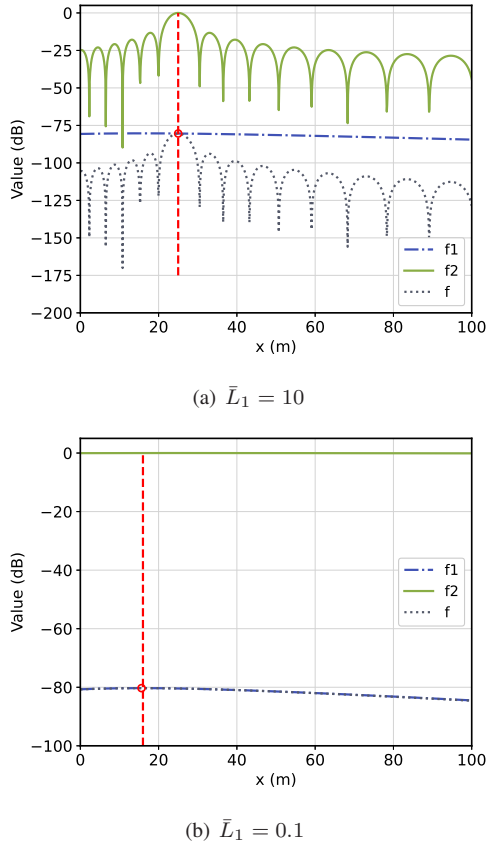


Fig. 3. Values of $f(x)$, $f_1(x)$ and $f_2(x)$ versus the placement position x , where the red circle and red dashed line indicate the optimal placement positions obtained by the closed-form and numerical result, respectively.

this case, the placement position x is designed to maximize $f_1(x)$. The problem can be equivalently formulated as

$$\min_x \left((x - x_t)^2 + y_t^2 \right) \left((x_r - x)^2 + y_r^2 \right). \quad (12)$$

Lemma 1: The optimal solution to (12) can be obtained by solving the following equation

$$a_c x^3 + b_c x^2 + c_c x + d_c = 0, \quad (13)$$

where $a_c = 3$, $b_c = -(5x_t + 4x_r)$, $c_c = (x_r^2 + y_r^2) + 2(x_t^2 + y_t^2) + 6x_r x_t$, and $d_c = -[(x_r^2 + y_r^2)x_t + 2(x_t^2 + y_t^2)x_r]$, respectively.

Proof: Please refer to Appendix B. ■

Since (13) is a cubic equation, it can be solved in closed-form. Then, the optimal placement position corresponds to the solution with the minimum objective function.

It is observed from Fig. 3 that the optimal placement positions obtained by the closed-form well match with those obtained by numerical results for both electrically large and small reflectors. Moreover, the reflector placement position optimization brings considerable performance gain of several tens of dB for electrically large reflectors. Such a significant gain motivates us to focus on electrically large reflectors in the following.

2) *Multi-MR Case:* Next, we consider the case of single target location power enhancement assisted by multiple MRs. In this case, problem (P1) is reduced to

$$\begin{aligned} \max_{\{x_m\}_{m=1}^M} & \sum_{m=1}^M f(x_m) \\ \text{s.t.} & |x_m - x_n| \geq d_{m,n}^{\min}, \forall m, n \in \mathcal{M}, m \neq n, \end{aligned} \quad (14)$$

where $d_{m,n}^{\min} = L_1$ corresponds to the minimum distance to avoid the overlaps of MRs.

Before solving (14), we first study the property of the function $g(\Delta) \triangleq \text{sinc}^2(\pi L \Delta)$. The null-to-null beam width can be obtained by letting $\pi L \Delta = \pm\pi$, which is given by $2/L$. The main lobe width is then defined as half of the null-to-null beam width, i.e., the range of main lobe is $[-\frac{1}{2L}, \frac{1}{2L}]$, and $G \triangleq g(\frac{1}{2L}) \approx 0.4$ is the value at the endpoint of the beamforming main lobe. Moreover, the value of $g(\Delta)$ monotonically decreases within the main lobe as $|\Delta|$ increases. Thus, for electrically large reflectors, the reflector should be placed such that the corresponding $|\Delta|$ is as small as possible.

Motivated by the above discussions, the placement positions of reflectors are designed such that the Rx is located within their beamforming main lobes. Specifically, for $f_2(x)$, the placement positions x corresponding to the boundary points of the beamforming main lobe can be obtained by letting $\frac{x_r - x}{d_r(x)} - \frac{x - x_t}{d_t(x)} = \pm \frac{1}{2L_1}$, and the solution can be found numerically, denoted as x_{br} and x_{bl} , respectively. It is worth mentioning that the projection Δ decreases as the reflector moves from the Tx to Rx, and thus $x_{br} < x_{bl}$. In particular, when the placement position is out of $[x_{br}, x_{bl}]$, the reflector contributes little to the receive power, and thus this case is not considered here. To ensure that $|\Delta(x_m)|$ of reflector m is as small as possible, the reflector m should be placed close to x^* given in (11). Thus, the actual number of reflectors to be deployed is

$$\tilde{M} = \left\lfloor \frac{x^* - x_{br}}{L_1} \right\rfloor + \left\lfloor \frac{x_{bl} - x^*}{L_1} \right\rfloor + 1, \quad (15)$$

and the placement position of reflector m , $1 \leq m \leq \tilde{M}$, is

$$x_m^* = x^* - \left\lfloor \frac{x^* - x_{br}}{L_1} \right\rfloor L_1 + (m - 1) L_1. \quad (16)$$

B. Area Coverage Enhancement

In this subsection, we consider the case of area coverage enhancement.

1) *Single-MR Case:* For the target area illustrated in Fig. 1, let $\mathbf{r}_{ul} = [x_c - D_x/2, y_c + D_y/2]^T$, $\mathbf{r}_{ul} = [x_c - D_x/2, y_c - D_y/2]^T$, $\mathbf{r}_{ur} = [x_c + D_x/2, y_c + D_y/2]^T$, and $\mathbf{r}_{lr} = [x_c + D_x/2, y_c - D_y/2]^T$ denote the upper left, lower left, upper right and lower right corners of \mathcal{A} , respectively. In the case of single-MR aided area coverage enhancement, problem (P1) becomes

$$\max_x \min_{\mathbf{r} \in \mathcal{A}} \sigma_{\max} f_1(x; \mathbf{r}) f_2(x; \mathbf{r}). \quad (17)$$

For any given reflector placement position x , let $\Delta_{\max}(x)$ and $\Delta_{\min}(x)$ denote the maximum and minimum projection values in the target area \mathcal{A} , given by

$$\Delta_{\max}(x) \triangleq \max_{\mathbf{r} \in \mathcal{A}} \frac{x_r - x}{\sqrt{(x_r - x)^2 + y_r^2}} - \frac{x - x_t}{\sqrt{(x - x_t)^2 + y_t^2}}, \quad (18)$$

$$\Delta_{\min}(x) \triangleq \min_{\mathbf{r} \in \mathcal{A}} \frac{x_r - x}{\sqrt{(x_r - x)^2 + y_r^2}} - \frac{x - x_t}{\sqrt{(x - x_t)^2 + y_t^2}}. \quad (19)$$

For electrically large reflector, problem (17) is approximated as

$$\max_x \min_{\Delta_{\min}(x) \leq \Delta \leq \Delta_{\max}(x)} f_2(x; \Delta) \triangleq \text{sinc}^2(\pi \bar{L}_1 \Delta). \quad (20)$$

The null points of $f_2(x; \Delta)$ can be obtained by letting $\pi \bar{L}_1 \Delta = \pm z \pi$, $z \in \mathcal{N}_+$, i.e., $\Delta = \pm z / \bar{L}_1$. For any given placement position x , if there exist one or more null points in the range $[\Delta_{\min}(x), \Delta_{\max}(x)]$, the minimum value within the target area is zero. Otherwise, the minimum value in the target area occurs at $\Delta_{\min}(x)$ or $\Delta_{\max}(x)$. Thus, we have

$$\min_{\Delta_{\min}(x) \leq \Delta \leq \Delta_{\max}(x)} \text{sinc}^2(\pi \bar{L}_1 \Delta) = \begin{cases} 0, & \text{if } \exists z \in \mathcal{N}_+, \text{ s.t. } \pm z / \bar{L}_1 \in [\Delta_{\min}(x), \Delta_{\max}(x)], \\ \min \{ \text{sinc}^2(\pi \bar{L}_1 \Delta_{\min}(x)), \text{sinc}^2(\pi \bar{L}_1 \Delta_{\max}(x)) \}, & \text{otherwise.} \end{cases} \quad (21)$$

With (21), the optimal solution to (20) can be effectively obtained via the one-dimensional search. Furthermore, the search region can be reduced by noting that the specular reflection direction should point towards the target area. Specifically, as the reflector moves towards the target area, the specular reflection direction first points towards the lower left corner of \mathcal{A} , i.e., \mathbf{r}_{ll} , and finally points towards the upper right corner, i.e., \mathbf{r}_{ur} . The minimum and maximum placement positions are then determined by regarding the lower left and upper right corners as the single target location, respectively. With Proposition 1, we have

$$x_{\text{lower}} = x_t + \frac{y_t}{y_t + y_c - \frac{D_y}{2}} \left(x_c - \frac{D_x}{2} - x_t \right), \quad (22)$$

$$x_{\text{upper}} = x_t + \frac{y_t}{y_t + y_c + \frac{D_y}{2}} \left(x_c + \frac{D_x}{2} - x_t \right). \quad (23)$$

Thus, the search region of the placement is reduced to $[x_{\text{lower}}, x_{\text{upper}}]$. The main procedures for solving problem (20) are summarized in Algorithm 1.

2) *Multi-MR Case*: Furthermore, we consider the case of area coverage enhancement with multiple MRs. The receive power at any location \mathbf{r} within \mathcal{A} can be expressed as

$$P_r(\mathbf{r}) = \sum_{m=1}^M \frac{P_t \lambda^2}{(4\pi)^3} \sigma_{\max} f_1(x_m; \mathbf{r}) f_2(x_m; \mathbf{r}). \quad (24)$$

For electrically large reflector, problem (P1) is approximated as

$$\begin{aligned} \max_{\{x_m\}_{m=1}^M} \min_{\mathbf{r} \in \mathcal{A}} \sum_{m=1}^M f_2(x_m; \mathbf{r}) \\ \text{s.t. } |x_m - x_n| \geq L_1, \forall m, n \in \mathcal{M}, m \neq n. \end{aligned} \quad (25)$$

Algorithm 1 Reflector Placement Position Optimization for (20)

- 1: **Initialization**: Set the region of the reflector placement position $x \in [x_{\text{lower}}, x_{\text{upper}}]$ based on (22) and (23).
 - 2: For any candidate placement position x , calculate the maximum projection value $\Delta_{\max}(x)$ and the minimum projection value $\Delta_{\min}(x)$ based on (18) and (19), respectively.
 - 3: Obtain the minimum value of $\text{sinc}^2(\pi \bar{L}_1 \Delta)$ within \mathcal{A} based on (21).
 - 4: Choose the x that gives the maximum value in (20) as the optimal placement position.
-

Even for the simplified problem (25), it is still difficult to be directly solved. To tackle this issue, we propose a sequential placement algorithm, where any location of the target area can be covered by the beamforming main lobe of one reflector.

Let x_m^* denote the optimized placement position of MR m , and $\mathbf{r}_{m,l}$ and $\mathbf{r}_{m,r}$ denote the locations corresponding to left and right endpoints of the beamforming main lobe with respect to (w.r.t.) MR m , respectively, as illustrated in Fig. 11 in the appendix. For the proposed sequential placement algorithm, the parameters are determined in the following order,

$$\mathbf{r}_{1,r} \rightarrow x_1^* \rightarrow \mathbf{r}_{1,l}(\mathbf{r}_{2,r}) \rightarrow x_2^* \rightarrow \mathbf{r}_{2,l}(\mathbf{r}_{3,r}) \rightarrow \dots \quad (26)$$

Specifically, by choosing the upper right corner \mathbf{r}_{ur} as the location corresponding to the right endpoint of the beamforming main lobe w.r.t. the first MR, we have $\mathbf{r}_{1,r} = \mathbf{r}_{ur}$. Then, for MR m , the placement position x_m is designed such that $\Delta(x_m; \mathbf{r}_{m,r}) = \frac{1}{2\bar{L}_1}$, i.e.,

$$\frac{x_{m,r} - x_m}{\sqrt{(x_{m,r} - x_m)^2 + y_{m,r}^2}} - \frac{x_m - x_t}{\sqrt{(x_m - x_t)^2 + y_t^2}} = \frac{1}{2\bar{L}_1}, \quad (27)$$

where $x_{m,r}$ and $y_{m,r}$ denote the x - and y -coordinate of $\mathbf{r}_{m,r}$, respectively, and the solution, x_m^* , can be obtained numerically. With x_m^* , the projection of \mathbf{r}_{ll} w.r.t. MR m , i.e., $\Delta(x_m^*; \mathbf{r}_{ll})$, is obtained. When $\Delta(x_m^*; \mathbf{r}_{ll}) \in \left[-\frac{1}{2\bar{L}_1}, \frac{1}{2\bar{L}_1}\right]$, the lower left corner can be covered by the beamforming main lobe of MR m , and the sequential placement is ended. Otherwise, the next MR is then deployed. To this end, the location corresponding to the left endpoint of the beamforming main lobe w.r.t. MR m needs to be determined, as shown in the following lemma.

Lemma 2: A location corresponding to the left endpoint of the beamforming main lobe w.r.t. MR m can be expressed as

$$\mathbf{r}_{m,l} = [x_{m,l}, y_{m,l}]^T = \begin{cases} \left[x_r, y_c + \frac{D_y}{2} \right]^T, & \text{if } \Delta(x_m^*; \mathbf{r}_{ul}) < -\frac{1}{2\bar{L}_1}, \\ \left[x_c - \frac{D_x}{2}, y_r \right]^T, & \text{if } \Delta(x_m^*; \mathbf{r}_{ul}) \geq -\frac{1}{2\bar{L}_1} \text{ and} \\ & \Delta(x_m^*; \mathbf{r}_{ll}) < -\frac{1}{2\bar{L}_1}, \end{cases} \quad (28)$$

where x_r and y_r are the values within $(x_c - D_x/2, x_c + D_x/2)$ and $(y_c - D_y/2, y_c + D_y/2)$, respectively, and

Algorithm 2 Sequential Placement Algorithm for Solving (25)

- 1: Initialize $\mathbf{r}_{1,r} = \mathbf{r}_{ur}$, and let $m = 1$.
 - 2: **repeat**
 - 3: For given $\mathbf{r}_{m,r}$, solve the equation (27), and denote the solution as x_m^* .
 - 4: For given x_m^* , solve the equation (29), and denote the solution as $\mathbf{r}_{m,l}$.
 - 5: $\mathbf{r}_{m+1,r} = \mathbf{r}_{m,l}$.
 - 6: Update $m = m + 1$.
 - 7: **until** \mathbf{r}_{ll} is covered by the beamforming main lobe of one MR.
-

$\Delta(x_m^*, \mathbf{r}_{ul})$ denotes the projection of the upper left corner \mathbf{r}_{ul} w.r.t. MR m .

Proof: Please refer to Appendix C. ■

Furthermore, the unknown parameter in Lemma 2 can be obtained by solving the equation $\Delta(x_m^*, \mathbf{r}_{m,l}) = -\frac{1}{2L_1}$, i.e.,

$$\frac{x_{m,l} - x_m^*}{\sqrt{(x_{m,l} - x_m^*)^2 + y_{m,l}^2}} - \frac{x_m^* - x_t}{\sqrt{(x_m^* - x_t)^2 + y_t^2}} = -\frac{1}{2L_1}. \quad (29)$$

Subsequently, the $(m+1)$ -th MR is placed such that $\mathbf{r}_{m,l}$ is covered by the right endpoint of the beamforming main lobe w.r.t. MR $m+1$, i.e., $\mathbf{r}_{m+1,r} = \mathbf{r}_{m,l}$. Similarly, the parameters x_{m+1}^* and $\mathbf{r}_{m+1,l}$ can be obtained. Note that when $|x_{m+1}^* - x_m^*| \geq L_1$, the placement strategy constitutes a feasible solution. Otherwise, one cannot find a solution to ensure that any location of the target area is covered by the beamforming main lobe of one MR.

Finally, the sequential placement is completed until the lower left corner \mathbf{r}_{ll} is located within the beamforming main lobe of one reflector. The main procedures of the proposed sequential placement algorithm are summarized in Algorithm 2.

IV. FLEXIBLE REFLECTOR

In this section, we study the general FR-aided coverage enhancement.

A. Single Target Location Power Enhancement

1) *Single-FR Case:* For the single target location power enhancement by a single-FR, we have

$$f(x, \omega) = \frac{\sigma(x, \omega)}{d_t^2(x) d_r^2(x)} = \sigma_{\max} \times \underbrace{\frac{\eta(x, \omega)}{d_t^2(x) d_r^2(x)}}_{f_1(x, \omega)} \underbrace{\text{sinc}^2(\pi \bar{L}_1 \Delta(x, \omega))}_{f_2(x, \omega)}, \quad (30)$$

and problem (P1) is reduced to

$$\begin{aligned} \max_{x, \omega} \quad & f(x, \omega) \\ \text{s.t.} \quad & (\mathbf{a}_t^T(x) \mathbf{n}(\omega)) (\mathbf{a}_r^T(x) \mathbf{n}(\omega)) < 0, \end{aligned} \quad (31)$$

where the notation of location \mathbf{r} is omitted.

To tackle the non-convex problem (31), for any given placement position x , the rotation angle is optimized to maximize the following problem

$$\begin{aligned} \max_{\omega} \quad & \text{sinc}^2(\pi \bar{L}_1 \Delta(x, \omega)) \\ \text{s.t.} \quad & (\mathbf{a}_t^T(x) \mathbf{n}(\omega)) (\mathbf{a}_r^T(x) \mathbf{n}(\omega)) < 0. \end{aligned} \quad (32)$$

Then, by substituting the obtained solution, denoted as $\omega^*(x)$, into the objective function of (31), the placement position optimization yields the following problem

$$\max_x f(x, \omega^*(x)). \quad (33)$$

Proposition 2: An optimal solution to problem (32) is

$$\omega^*(x) = \arctan \left(-\frac{\frac{1}{d_r(x)}(x_r - x) - \frac{1}{d_t(x)}(x - x_t)}{\frac{1}{d_r(x)}y_r + \frac{1}{d_t(x)}y_t} \right). \quad (34)$$

Proof: Please refer to Appendix D. ■

Note that after rotation by angle $\omega^*(x)$, the new incident angle is $\tilde{\theta}_t = \theta_t + \omega^*(x)$, and $\cos(\tilde{\theta}_t) = \frac{-\mathbf{a}_t^T(x) \mathbf{n}(\omega^*(x))}{\|\mathbf{a}_t(x)\| \|\mathbf{n}(\omega^*(x))\|} = -\frac{\mathbf{a}_t^T(x) \mathbf{a}_r(x) - 1}{\|\mathbf{a}_r(x) - \mathbf{a}_t(x)\|}$. Besides, the new reflection angle is $\tilde{\theta}_r = \theta_r - \omega^*(x)$, and $\cos(\tilde{\theta}_r) = \frac{\mathbf{a}_r^T(x) \mathbf{n}(\omega^*(x))}{\|\mathbf{a}_r(x)\| \|\mathbf{n}(\omega^*(x))\|} = -\frac{\mathbf{a}_r^T(x) \mathbf{a}_r(x) - 1}{\|\mathbf{a}_r(x) - \mathbf{a}_t(x)\|}$. Thus, we have $\cos(\tilde{\theta}_t) = \cos(\tilde{\theta}_r)$, i.e., simple rotation achieves the manipulation of specular direction pointing towards the Rx.

With the rotation angle (34), and after some manipulations, the objective function in (31) is reduced to

$$\begin{aligned} f(x, \omega^*(x)) &= \sigma_{\max} f_1(x, \omega^*(x)) = \sigma_{\max} \frac{\eta(x, \omega^*(x))}{d_t^2(x) d_r^2(x)} \\ &= \sigma_{\max} \frac{\cos^2(\theta_r - \omega^*(x))}{d_t^2(x) d_r^2(x)} = \sigma_{\max} \frac{\|\mathbf{a}_r(x) - \mathbf{a}_t(x)\|^2}{4d_t^2(x) d_r^2(x)}. \end{aligned} \quad (35)$$

Thus, problem (33) can be equivalently expressed as

$$\max_x \frac{\|\mathbf{a}_r(x) - \mathbf{a}_t(x)\|^2}{4d_t^2(x) d_r^2(x)}. \quad (36)$$

Since the resulting objective function is a highly complicated function w.r.t. placement position x , the one-dimensional search is applied to efficiently obtain the optimal FR placement position x_{FR}^* .

2) *Multi-FR Case:* For multi-FR aided single target location power enhancement, problem (P1) is reduced to

$$\max_{\{x_m, \omega_m\}_{m=1}^M} \sum_{m=1}^M f(x_m, \omega_m) \quad (37)$$

$$\text{s.t.} \quad |x_m - x_n| \geq d_{m,n}^{\min}, \quad \forall m, n \in \mathcal{M}, m \neq n,$$

$$(\mathbf{a}_t^T(x_m) \mathbf{n}(\omega_m)) (\mathbf{a}_r^T(x_m) \mathbf{n}(\omega_m)) < 0, \quad \forall m, \mathbf{r}.$$

To solve this problem, we first analyze the minimum distance to avoid the signal blockage, given in the following lemma.

Lemma 3: For any given placement position and rotation angle pair (x, ω) , the minimum distance to avoid the signal blockage is

$$d(x, \omega) = \begin{cases} L_1, & \text{if } \omega = 0. \\ \max(d_i(x, \omega), d_r(x, \omega)), & \text{otherwise,} \end{cases} \quad (38)$$

Algorithm 3 Multi-FR Design for Solving (37)

- 1: Initialize $\Omega = \emptyset$, $x_1^+ = x_1^- = x_{\text{FR}}^*$, and let $i = j = 1$.
 - 2: **while** $i \leq \lceil (M + 1) / 2 \rceil$
 - 3: $\Omega = \Omega \cup x_i^+$.
 - 4: Calculate $\omega^*(x_i^+)$ based on (34).
 - 5: $x_{i+1}^+ = x_i^+ + d(x_i^+, \omega^*(x_i^+))$.
 - 6: Update $i = i + 1$.
 - 7: **end while**
 - 8: **while** $j \leq \lceil (M + 1) / 2 \rceil$
 - 9: $\Omega = \Omega \cup x_j^-$.
 - 10: Calculate $\omega^*(x_j^-)$ based on (34).
 - 11: $x_{j+1}^- = x_j^- - d(x_j^-, \omega^*(x_j^-))$.
 - 12: Update $j = j + 1$.
 - 13: **end while**
 - 14: $\Omega = \Omega \setminus x_{\text{FR}}^*$.
 - 15: Calculate the objective function values (35) of all candidate placement positions within Ω .
 - 16: Select the placement positions with M largest values as the optimized FR placement positions.
-

where $d_i(x, \omega) \triangleq \frac{L_1}{2} \left(\cos \omega - \tan \theta_t \sin \omega + \frac{1}{\cos \theta_t} \right)$ and $d_r(x, \omega) \triangleq \frac{L_1}{2} \left(\cos \omega + \tan \theta_r \sin \omega + \frac{1}{\cos \theta_r} \right)$, respectively.

Proof: Please refer to Appendix E. \blacksquare

Then, the deployment of multi-FR will utilize the result given in Section IV-A1, i.e., FRs are placed close to x_{FR}^* , without giving rise to the signal blockage. Meanwhile, the rotation angle of each FR is adjusted such that the reflective beamforming points towards the Rx. Let Ω denote the set of candidate placement positions for the deployed FRs. The main procedures are summarized in Algorithm 3.

B. Area Coverage Enhancement

In this subsection, we consider the FR-aided area coverage enhancement.

1) *Single-FR Case:* For the single-FR aided area coverage enhancement, problem (P1) becomes

$$\begin{aligned} \max_{x, \omega} \min_{\mathbf{r} \in \mathcal{A}} f(x, \omega; \mathbf{r}) \\ \text{s.t. } (\mathbf{a}_t^T(x) \mathbf{n}(\omega)) (\mathbf{a}_r^T(x; \mathbf{r}) \mathbf{n}(\omega)) < 0, \forall \mathbf{r}. \end{aligned} \quad (39)$$

Similar to Section III-B1, for any given placement position x and rotation angle ω , the maximum and minimum projection values within \mathcal{A} are respectively defined as

$$\Delta_{\max}(x, \omega) \triangleq \max_{\mathbf{r} \in \mathcal{A}} (\mathbf{a}_r(x; \mathbf{r}) - \mathbf{a}_t(x))^T \mathbf{u}(\omega), \quad (40)$$

$$\Delta_{\min}(x, \omega) \triangleq \min_{\mathbf{r} \in \mathcal{A}} (\mathbf{a}_r(x; \mathbf{r}) - \mathbf{a}_t(x))^T \mathbf{u}(\omega). \quad (41)$$

In the following, we propose an efficient rotation design. Specifically, for any given placement position x , the maximum and minimum projection values without rotation (i.e., $\omega = 0$) can be obtained based on (18) and (19), respectively, with the corresponding area locations denoted as $\mathbf{r}_{\max}(x)$ and $\mathbf{r}_{\min}(x)$, respectively. In order to balance the array factor within \mathcal{A} , the rotation angle is designed such that $\Delta(x, \omega; \mathbf{r}_{\max}(x)) =$

$-\Delta(x, \omega; \mathbf{r}_{\min}(x))$, i.e., the boundary points $\mathbf{r}_{\max}(x)$ and $\mathbf{r}_{\min}(x)$ enjoy the identical array factor. Thus, we have

$$(\mathbf{a}_r(x; \mathbf{r}_{\max}(x)) + \mathbf{a}_r(x; \mathbf{r}_{\min}(x)) - 2\mathbf{a}_t(x))^T \mathbf{u}(\omega) = 0. \quad (42)$$

Based on the result in Proposition 2, the rotation angle is given by $\omega(x) = \arctan\left(-\frac{[\mathbf{a}_r(x; \mathbf{r}_{\max}(x)) + \mathbf{a}_r(x; \mathbf{r}_{\min}(x)) - 2\mathbf{a}_t(x)]_1}{[\mathbf{a}_r(x; \mathbf{r}_{\max}(x)) + \mathbf{a}_r(x; \mathbf{r}_{\min}(x)) - 2\mathbf{a}_t(x)]_2}\right)$. Then, by substituting $\omega(x)$ into (40) and (41), the maximum and minimum projection values within \mathcal{A} for given placement position x and rotation angle $\omega(x)$ can be obtained, denoted as $\Delta_{\max}(x, \omega(x))$ and $\Delta_{\min}(x, \omega(x))$, respectively.

For electrically large FR, problem (39) is reduced to

$$\max_x \min_{\Delta_{\min}(x, \omega(x)) \leq \Delta \leq \Delta_{\max}(x, \omega(x))} f_2(x; \Delta). \quad (43)$$

The detail for solving (43) is similar to that for solving (20), which is omitted for brevity.

2) *Multi-FR Case:* For the case of area coverage with electrically large multiple FRs, problem (P1) is reduced to

$$\begin{aligned} \max_{\{x_m, \omega_m\}_{m=1}^M} \min_{\mathbf{r} \in \mathcal{A}} \sum_{m=1}^M f_2(x_m, \omega_m; \mathbf{r}) \\ \text{s.t. } |x_m - x_n| \geq d_{m,n}^{\min}, \forall m, n \in \mathcal{M}, m \neq n, \\ (\mathbf{a}_t^T(x_m) \mathbf{n}(\omega_m)) (\mathbf{a}_r^T(x_m; \mathbf{r}) \mathbf{n}(\omega_m)) < 0, \forall m, \mathbf{r}. \end{aligned} \quad (44)$$

Motivated by the multi-MR design in Section III-B2, we propose a sequential placement and rotation design. Let x_m^* and ω_m^* denote the optimized placement position and rotation angle of FR m , and $\mathbf{r}_{m,l}$ and $\mathbf{r}_{m,r}$ follow the same definitions as in Section III-B2. The parameters are then determined in the following order,

$$\mathbf{r}_{1,r} \rightarrow x_1^* \rightarrow \omega_1^* \rightarrow \mathbf{r}_{1,l}(\mathbf{r}_{2,r}) \rightarrow x_2^* \rightarrow \omega_2^* \rightarrow \dots \quad (45)$$

Specifically, by letting $\mathbf{r}_{1,r} = \mathbf{r}_{ur}$, the placement position of the first FR is designed such that the concatenated path loss from the Tx to $\mathbf{r}_{1,r}$ is minimized, i.e.,

$$x_1^* = \arg \min_x f_{\text{pl}}(x; \mathbf{r}_{1,r}) \triangleq d_t^2(x) d_r^2(x; \mathbf{r}_{1,r}). \quad (46)$$

Then, for FR m , when the placement position x_m^* is obtained, the rotation angle ω_m is designed such that

$$\Delta(x_m^*, \omega_m; \mathbf{r}_{m,r}) = \frac{1}{2L_1}. \quad (47)$$

The solution to (47) can be obtained numerically and denoted as ω_m^* . Furthermore, one location corresponding to the left endpoint of the beamforming main lobe w.r.t. FR m can be determined by solving the following equation,

$$\Delta(x_m^*, \omega_m^*; \mathbf{r}_{m,l}) = -\frac{1}{2L_1}. \quad (48)$$

Subsequently, the placement position of FR $m + 1$ is selected to reduce the concatenated path loss from the Tx to $\mathbf{r}_{m+1,r} = \mathbf{r}_{m,l}$, and its rotation angle is designed such that $\mathbf{r}_{m,l}$ is covered by the right endpoint of the beamforming main lobe w.r.t. FR $m + 1$. Finally, the sequential placement and rotation design is ended until the lower left corner \mathbf{r}_{ll} is covered by the beamforming main lobe of one FR. The main procedures are summarized in Algorithm 4.

Algorithm 4 Sequential Placement and Rotation Algorithm for Solving (44)

- 1: Initialize $\mathbf{r}_{1,r} = \mathbf{r}_{ur}$, and let $m = 1$.
 - 2: Obtain the optimized placement position of FR 1 based on (46).
 - 3: **repeat**
 - 4: For given $\mathbf{r}_{m,r}$ and x_m^* , solve the equation (47), and denote the solution as ω_m^* .
 - 5: For given x_m^* and ω_m^* , solve the equation (48), and denote the solution as $\mathbf{r}_{m,l}$.
 - 6: $\mathbf{r}_{m+1,r} = \mathbf{r}_{m,l}$.
 - 7: **if** $m = 1$
 - 8: $x_{m+1}^- = x_m^* - d(x_m^*, \omega_m^*)$.
 - 9: $x_{m+1}^+ = x_m^* + d(x_m^*, \omega_m^*)$.
 - 10: **else**
 - 11: **if** $x_m^* = x_m^-$
 - 12: $x_{m+1}^- = x_m^* - d(x_m^*, \omega_m^*)$.
 - 13: $x_{m+1}^+ = x_m^+$.
 - 14: **else**
 - 15: $x_{m+1}^- = x_m^-$.
 - 16: $x_{m+1}^+ = x_m^* + d(x_m^*, \omega_m^*)$.
 - 17: **end if**
 - 18: **end if**
 - 19: **if** $f_{pl}(x_{m+1}^-; \mathbf{r}_{m+1,r}) \leq f_{pl}(x_{m+1}^+; \mathbf{r}_{m+1,r})$
 - 20: $x_{m+1}^* = x_{m+1}^+$.
 - 21: **else**
 - 22: $x_{m+1}^* = x_{m+1}^-$.
 - 23: **end if**
 - 24: Update $m = m + 1$.
 - 25: **until** \mathbf{r}_{ul} is covered by the beamforming main lobe of one FR.
-

V. NUMERICAL RESULTS

In this section, numerical results are provided to evaluate the proposed MR and FR designs. Unless otherwise stated, the carrier frequency is $f_c = 2.4$ GHz. The wavelength-normalized length and width of the reflector are $\bar{L}_1 = 10$ and $\bar{L}_2 = 5$, respectively.

A. Single Target Location

Fig. 4 shows the receive power of the Rx versus the placement position x for MR, where the locations of the Tx and Rx are $\mathbf{t} = [0, -50]^T$ m and $\mathbf{r} = [100, -150]^T$ m, respectively. It is observed that the receive power exhibits significant variations as the placement position changes, and the performance gap between the maximum and minimum receive power is up to tens of dBm. This demonstrates the necessity of placement optimization for MR. It is also observed that when $\bar{L}_1 \gg 1$, the derived placement position in (11) gives a quite accurate approximation of the optimal placement position to maximize the receive power at the Rx.

Fig. 5 shows the receive power versus the placement position x and rotation angle ω for FR, where the receive power below -160 dBm is truncated to -160 dBm for convenience of presentation. It is observed that a significant performance gain can be achieved by adjusting the placement position and

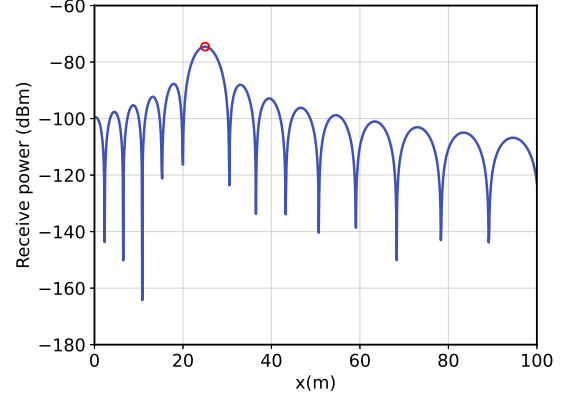


Fig. 4. The receive power versus the placement position x for single-MR aided single target location power enhancement, where the placement position given in (11) is marked by the red circle.

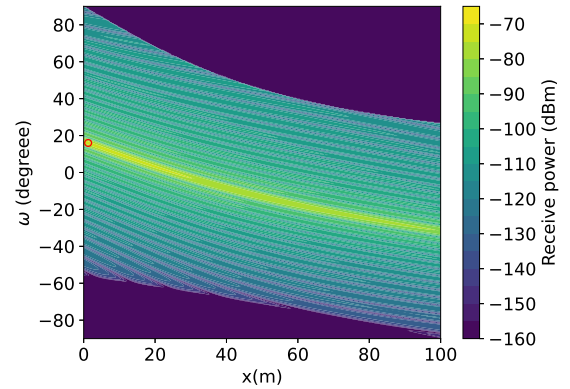


Fig. 5. The receive power versus the placement position x and rotation angle ω for single-FR aided single target location power enhancement, where the optimal placement position and rotation angle pair (x^*, ω^*) is marked by the red circle.

rotation angle. Moreover, for the considered setup, different from the MR that is placed at the specular reflection point, the FR is preferable to deploy in the vicinity of x -coordinate of the Tx.

Fig. 6 shows the receive power versus the movable region size. For comparison, the following two benchmark schemes are considered: 1) Fixed-position reflector (FPR): the reflector placement position is fixed at $x = x_t$; 2) Fixed-position rotatable reflector (FPRR): the reflector is capable of adjusting the rotation angle, while its placement position is fixed at $x = x_t$. The locations of the Tx and Rx are $\mathbf{t} = [0, -150]^T$ m and $\mathbf{r} = [100, -60]^T$ m, respectively. It is observed that the FR achieves the best performance, and the receive power for both the FR and MR improves as the movable region size increases. This is expected since the MR is of high probability to move to the specular point for a larger movable region size, and the FR is more likely to be close to the optimal placement position. By contrast, the receive power for both the FPR and FPRR remains unchanged as the region size increases, which is due to the fact that the FPR and FPRR cannot exploit the spatial design DoF of placement.

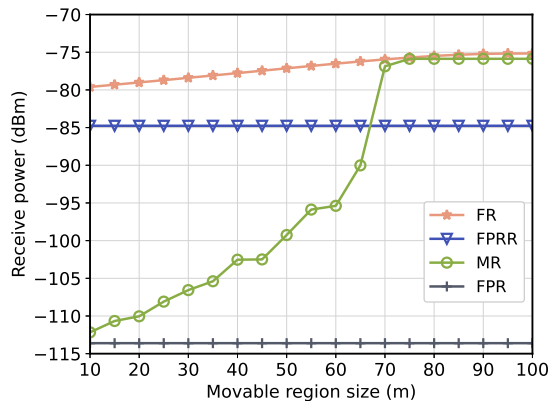


Fig. 6. The receive power versus the movable region size.

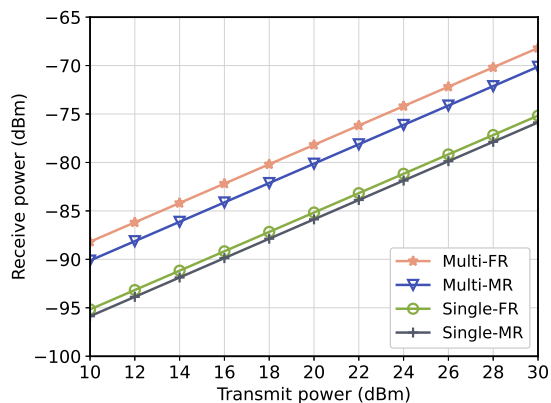


Fig. 7. The receive power versus the transmit power for multi-MR and multi-FR aided single target location power enhancement.

Moreover, the FPRR yields a much higher receive power than FPR, thanks to the additional rotation angle adjustment. In particular, considerable performance gain is achieved by FPRR over the MR for a relatively small movable region size, which may provide a satisfied scheme for the case of the restricted movable region.

As a further comparison, Fig. 7 shows the receive power versus the transmit power. For the cases of multi-MR and multi-FR, the number of reflectors is $M = 5$. It is observed that multi-FR achieves a higher receive power than single-FR, and a similar result can be observed for the case of MR. This is due to the fact that more power is captured and reflected by multiple reflectors. It is also observed that compared to the case of the single reflector, the performance gain of FR over MR is more significant in the case of multiple reflectors. This is expected since the multi-FR is able to obtain the full array factor at multiple placement positions, by flexibly adjusting the rotation angle.

B. Area Coverage Enhancement

Fig. 8 shows the minimum receive power versus the length of the target area D_x by considering the single reflector, where the receive power below -130 dBm is truncated to -130 dBm

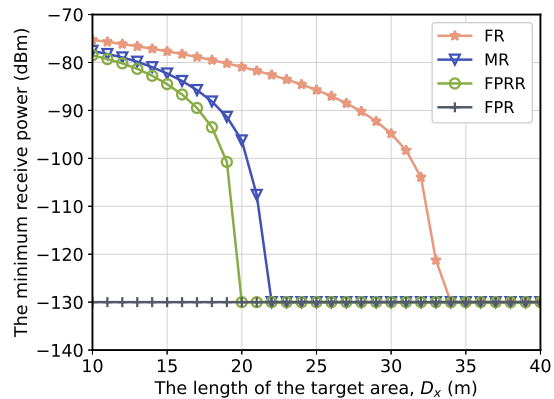


Fig. 8. The minimum receive power versus the length of the target area.

for convenience of presentation. The center of the target area is $\mathbf{r}_c = [100, -75]^T$ m, and its width is fixed as $D_y = 10$ m. The location of the Tx is $\mathbf{t} = [0, -50]^T$ m. The benchmark schemes of FPR and FPRR are considered, where the reflector is placed above the midpoint between the Tx and area center, i.e., $x = (x_t + x_c) / 2$. It is observed that the minimum receive power of the FR outperforms those of other three schemes for a relatively small area length, thanks to its flexible placement and rotation adjustment. Besides, the minimum receive power of FPR is always equal to zero (i.e., -130 dBm), this is because its null-to-null beam cannot cover the whole target area. It is also observed that as D_x increases, the minimum receive power of FPRR, MR and FR decreases and eventually drops to zero successively. The above result indicates that the FR is able to increase the coverage area size as compared to other three schemes, by fully exploiting the spatial design DoFs of placement and rotation.

Fig. 9 shows the reflection gain at different Rx locations for multi-MR aided area coverage enhancement, where the reflection gain at location \mathbf{r} is defined as $\sum_{m=1}^M f_2(x_m; \mathbf{r})$. The center of the target area is $\mathbf{r}_c = [100, -150]^T$ m, and its length and width are $D_x = 100$ m and $D_y = 50$ m, respectively. For comparison, the benchmark scheme where the reflectors are equally placed within the range $[x_t, x_r + D_x/2]$ is considered. Based on Algorithm 2, the number of required reflector is $M = 7$. It is observed from Fig. 9(a) that for the proposed sequential placement scheme in Algorithm 2, any location of the target area enjoys a reflection gain larger than 0.4, which is value of the endpoint of the beamforming main lobe. This implies that with the proposed sequential placement algorithm, any location of the target area can be covered by the beamforming main lobe of at least one reflector. By contrast, for the benchmark scheme, there exist many coverage holes with zero reflection gain, as can be seen in Fig. 9(b).

Fig. 10 shows the cumulative distribution function (CDF) of the receive power within the target area for the case of multiple reflectors. The number of MRs and FRs required for coverage are 7 and 6, respectively. As a comparison, the benchmark scheme of multi-MR in Fig. 9 is considered. For the benchmark scheme of multi-FR, the FRs are equally placed

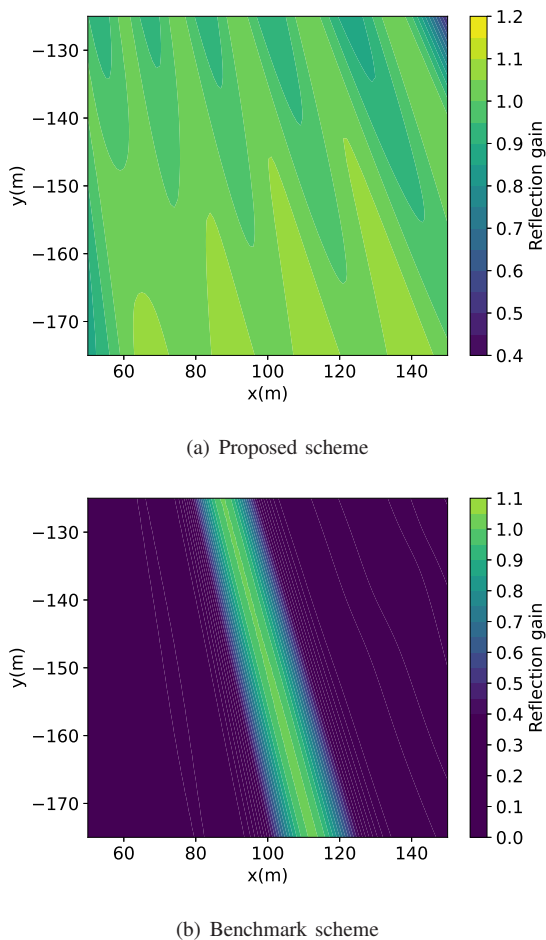


Fig. 9. Reflection gain at different Rx locations for multi-MR aided area coverage enhancement.

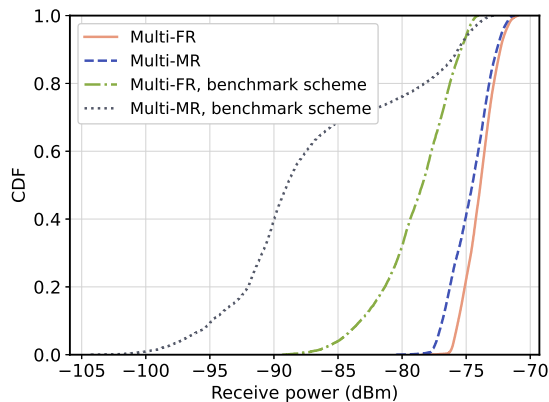


Fig. 10. The CDF of the receive power within the target area.

within $[x_t, x_r + D_x/2]$, and the rotation angles are designed similar to Algorithm 4. It is observed that the proposed multi-FR and multi-MR schemes are superior to their counterparts in the benchmark schemes, as expected. Moreover, FR in general yields a better area coverage performance compared to MR, even with a smaller number of reflectors, thanks to the additional design DoF of rotation.

VI. CONCLUSION

This paper proposed a new paradigm of passive reflective beamforming enabled by FR, which enables a flexible beamforming direction via both placement position and rotation angle adjustments. The minimum expected receive power over all locations within a given target area was maximized by jointly optimizing FRs' placement positions and rotation angles. To gain useful insights, the special case of MR was first considered by fixing its rotation angle, where the single- and multi-MR aided coverage enhancement were respectively studied. Moreover, the MR design was extended to the general case of the single- and multi-FR aided coverage enhancement. Numerical results showed that the proposed FR scheme significantly outperforms benchmark schemes in terms of receive power enhancement.

APPENDIX A PROOF OF PROPOSITION 1

When L_1 is much larger than the signal wavelength, the sinc function changes rapidly, as shown in Fig. 3(a). To this end, the optimization problem (10) can be approximated to maximize the array factor $f_2(x)$, yielding the following problem

$$\max_x \text{sinc}^2 \left(\pi \bar{L}_1 \left(\frac{x_r - x}{\|\mathbf{r} - \mathbf{q}\|} - \frac{x - x_t}{\|\mathbf{q} - \mathbf{t}\|} \right) \right). \quad (49)$$

It is known that the function $\text{sinc}(x)$ achieves the maximum value at $x = 0$. Thus, problem (49) can be maximized by letting $\frac{x_r - x}{\|\mathbf{r} - \mathbf{q}\|} - \frac{x - x_t}{\|\mathbf{q} - \mathbf{t}\|} = 0$. With $\mathbf{q} = [x, 0, 0]^T$, $\mathbf{t} = [x_t, y_t, 0]^T$ and $\mathbf{r} = [x_r, y_r, 0]^T$, we have

$$\frac{x_r - x}{\sqrt{(x_r - x)^2 + y_r^2}} - \frac{x - x_t}{\sqrt{(x - x_t)^2 + y_t^2}} = 0. \quad (50)$$

It can be seen that the solution x is within $[x_t, x_r]$. After some manipulations, we have

$$\frac{y_r}{x_r - x} = \frac{y_t}{x - x_t}, \quad (51)$$

and the optimal placement is

$$x^* = x_t + \frac{y_t}{y_t + y_r} (x_r - x_t). \quad (52)$$

This thus completes the proof of Proposition 1.

APPENDIX B PROOF OF LEMMA 1

Since the objective function of (12) is differentiable, the extreme points can be obtained by letting its first-order derivative w.r.t. x equal to zero, which yields

$$2 \left((x_r - x)^2 + y_r^2 \right) (a_c x^3 + b_c x^2 + c_c x + d_c) = 0, \quad (53)$$

where a_c , b_c , c_c , and d_c are given below (13). It is observed that $(x_r - x)^2 + y_r^2 > 0$, and thus (53) is equivalent to (13). The proof of Lemma 1 is thus completed.

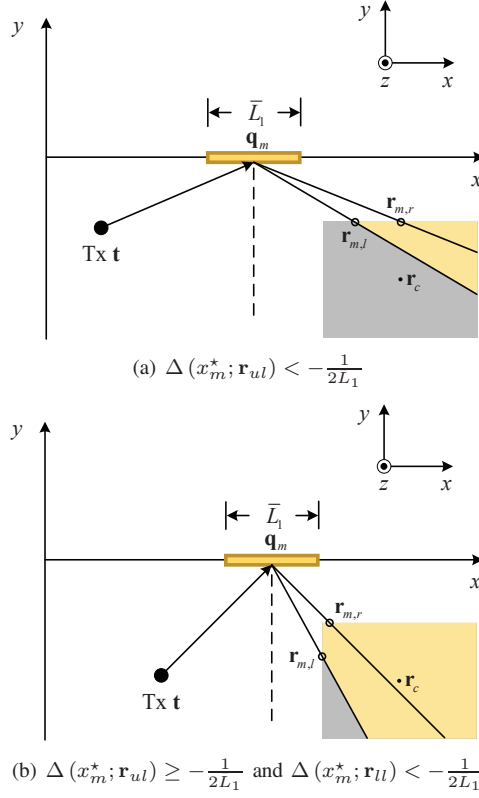


Fig. 11. An illustration of the coverage area, where the yellow part of the target area has been covered by the beamforming main lobes of the first m MRs, and $\mathbf{r}_{m,l}$ and $\mathbf{r}_{m,r}$ denote the locations corresponding to left and right endpoints of the beamforming main lobe w.r.t. MR m , respectively.

APPENDIX C PROOF OF LEMMA 2

Depending on the relationship between $\Delta(x_m^*; \mathbf{r}_{ul})$ and $-\frac{1}{2L_1}$, we have the following two cases.

Case 1: $\Delta(x_m^*; \mathbf{r}_{ul}) < -\frac{1}{2L_1}$, i.e., the upper left corner \mathbf{r}_{ul} is not covered by the beamforming main lobe of MR m , as illustrated in Fig. 11(a). Then, a location corresponding to the left endpoint of the beamforming main lobe is chosen as $[x_r, y_c + D_y/2]^T$, where $x_c - D_x/2 < x_r < x_c + D_x/2$.

Case 2: $\Delta(x_m^*; \mathbf{r}_{ul}) \geq -\frac{1}{2L_1}$ and $\Delta(x_m^*; \mathbf{r}_{ll}) < -\frac{1}{2L_1}$, i.e., the upper left corner \mathbf{r}_{ul} is covered by the beamforming main lobe of MR m , as illustrated in Fig. 11(b). In this case, a location corresponding to the left endpoint of the beamforming main lobe is chosen as $[x_c - D_x/2, y_r]^T$, where $y_c - D_y/2 < y_r < y_c + D_y/2$.

By combining the above two cases, the proof of Lemma 2 is thus completed.

APPENDIX D PROOF OF PROPOSITION 2

Since the objective function of problem (32) is maximized when $\Delta(x, \omega) = 0$, we show that for any given placement position x , there always exists a rotation angle satisfying the constraint of (32) such that $\Delta(x, \omega) = 0$. Specifically, to ensure that $\Delta(x, \omega) = 0$, we have

$$[\mathbf{a}_r(x) - \mathbf{a}_t(x)]_1 \cos \omega + [\mathbf{a}_r(x) - \mathbf{a}_t(x)]_2 \sin \omega = 0, \quad (54)$$

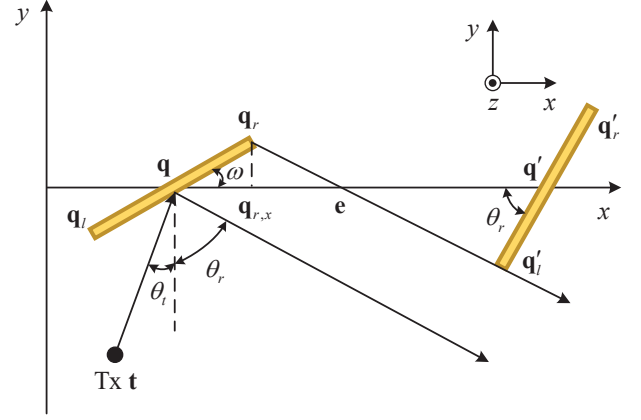


Fig. 12. A illustration of the minimum distance to ensure that the signal reflected by any location of the FR can reach the Rx.

where $[\mathbf{a}_r(x) - \mathbf{a}_t(x)]_i$ denotes the i -th element of the deflection vector $(\mathbf{a}_r(x) - \mathbf{a}_t(x))$. A solution to (54) can be obtained by letting

$$\begin{cases} \cos \omega = -\frac{[\mathbf{a}_r(x) - \mathbf{a}_t(x)]_2}{\|\mathbf{a}_r(x) - \mathbf{a}_t(x)\|}, \\ \sin \omega = \frac{[\mathbf{a}_r(x) - \mathbf{a}_t(x)]_1}{\|\mathbf{a}_r(x) - \mathbf{a}_t(x)\|}. \end{cases} \quad (55)$$

The rotation angle is then given by

$$\omega = \arctan\left(-\frac{[\mathbf{a}_r(x) - \mathbf{a}_t(x)]_1}{[\mathbf{a}_r(x) - \mathbf{a}_t(x)]_2}\right), \quad (56)$$

i.e., (34).

Moreover, with (56), the normal direction vector is

$$\mathbf{n}(\omega) = -\frac{\mathbf{a}_r(x) - \mathbf{a}_t(x)}{\|\mathbf{a}_r(x) - \mathbf{a}_t(x)\|}. \quad (57)$$

Thus, we have

$$\begin{aligned} \mathbf{a}_t^T(x) \mathbf{n}(\omega) &= -\frac{(\mathbf{a}_t^T(x) \mathbf{a}_r(x) - \mathbf{a}_t^T(x) \mathbf{a}_t(x))}{\|\mathbf{a}_r(x) - \mathbf{a}_t(x)\|} \\ &= -\frac{(\mathbf{a}_t^T(x) \mathbf{a}_r(x) - 1)}{\|\mathbf{a}_r(x) - \mathbf{a}_t(x)\|}. \end{aligned} \quad (58)$$

Since $\mathbf{a}_t^T(x) \mathbf{a}_r(x) < 1$, we have $\mathbf{a}_t^T(x) \mathbf{n}(\omega) > 0$. Similarly, $\mathbf{a}_r^T(x) \mathbf{n}(\omega) < 0$. Then, the rotation angle given in (56) achieves $\Delta(x, \omega) = 0$, while satisfying the constraint of (32). The proof of Proposition 2 is thus completed.

APPENDIX E PROOF OF LEMMA 3

The proof of Lemma 3 includes the following two cases.

Case 1: $\omega = 0$. In this case, the minimum distance to avoid the signal blockage is that avoids the overlap of reflectors, i.e., $d(x, \omega) = L_1$.

Case 2: $\omega \neq 0$. To avoid the signal blockage between adjacent FRs, the inter-FR distance should ensure that the signal from the Tx can reach any location of the FR, and the signal reflected by any location of the FR can reach the Rx. Specifically, we first derive the minimum distance to ensure that the signal reflected by any location of the FR can reach the

Rx. As illustrated in Fig. 12, for given FR with the placement position and rotation angle pair being (x, ω) , the location of the right endpoint is $\mathbf{q}_r = \mathbf{q} + [\frac{L_1}{2} \cos \omega, \frac{L_1}{2} \sin \omega]^T$. Denote by $\mathbf{q}_{r,x} = [x + \frac{L_1}{2} \cos \omega, 0]^T$ the projection point of \mathbf{q}_r onto the x -axis. For the standard uniform plane wave (UPW) model, let \mathbf{e} denote the intersection point between the x -axis and the signal arriving at the Rx via \mathbf{q}_r . Thus, to avoid the signal blockage, any location of another FR should locate above the straight line formed by \mathbf{q}_r and \mathbf{e} . In particular, the minimum distance satisfying the above condition occurs when $\mathbf{q}'_r - \mathbf{q}'_l$ is perpendicular to $\mathbf{q}'_l - \mathbf{q}_r$, as illustrated in Fig. 12. Thus, based on the geometric relationship, the minimum distance is given by $d_r(x, \omega) = \|\mathbf{e} - \mathbf{q}\| + \|\mathbf{q}' - \mathbf{e}\| = \frac{L_1}{2} \left(\cos \omega + \tan \theta_r \sin \omega + \frac{1}{\cos \theta_r} \right)$.

On the other hand, the minimum distance ensuring that the signal from the Tx can reach any location of the FR is similarly obtained, given by $d_i(x, \omega) = \frac{L_1}{2} \left(\cos \omega - \tan \theta_t \sin \omega + \frac{1}{\cos \theta_t} \right)$. The details are omitted for brevity. Thus, to minimum distance to avoid the signal blockage is $d(x, \omega) = \max(d_i(x, \omega), d_r(x, \omega))$.

By combining the above two cases, the proof of Lemma 3 is thus completed.

REFERENCES

- [1] H. Lu *et al.*, "A tutorial on near-field XL-MIMO communications towards 6G," *IEEE Commun. Surv. Tuts.*, vol. 26, no. 4, pp. 2213–2257, 4th Quart. 2024.
- [2] E. Björnson, L. Sanguinetti, H. Wymeersch, J. Hoydis, and T. L. Marzetta, "Massive MIMO is a reality – what is next?: Five promising research directions for antenna arrays," *Digit. Signal Process.*, vol. 94, pp. 3–20, Nov. 2019.
- [3] Z. Wang, J. Zhang, H. Du, W. E. I. Sha, B. Ai, D. Niyato, and M. Debbah, "Extremely large-scale MIMO: Fundamentals, challenges, solutions, and future directions," *IEEE Wireless Commun.*, vol. 31, no. 3, pp. 117–124, Jun. 2024.
- [4] "Framework and overall objectives of the future development of IMT for 2030 and beyond," ITU-R, DRAFT NEW RECOMMENDATION, Jun. 2023.
- [5] Y. Han, S. Jin, M. Matthaiou, T. Q. S. Quek, and C.-K. Wen, "Towards extra large-scale MIMO: New channel properties and low-cost designs," *IEEE Internet Things J.*, vol. 10, no. 16, pp. 14 569–14 594, Aug. 2023.
- [6] H. Wang and Y. Zeng, "Can sparse arrays outperform collocated arrays for future wireless communications?" in *Proc. IEEE GLOBECOM Workshops (GC Wkshps)*, 2023, pp. 667–672.
- [7] H. Wang, C. Feng, Y. Zeng, S. Jin, C. Yuen, B. Clerckx, and R. Zhang, "Enhancing spatial multiplexing and interference suppression for near- and far-field communications with sparse MIMO," *arXiv preprint arXiv:2408.01956*, 2024.
- [8] H. Lu, Y. Zeng, S. Jin, and R. Zhang, "Group movable antenna with flexible sparsity: Joint array position and sparsity optimization," *IEEE Wireless Commun. Lett.*, vol. 13, no. 12, pp. 3573–3577, Dec. 2024.
- [9] X. Li, H. Min, Y. Zeng, S. Jin, L. Dai, Y. Yuan, and R. Zhang, "Sparse MIMO for ISAC: New opportunities and challenges," *IEEE Wireless Commun.*, 2024.
- [10] P. Pal and P. P. Vaidyanathan, "Nested arrays: A novel approach to array processing with enhanced degrees of freedom," *IEEE Trans. Signal Process.*, vol. 58, no. 8, pp. 4167–4181, Aug. 2010.
- [11] M. Wang and A. Nehorai, "Coarrays, MUSIC, and the Cramér–Rao bound," *IEEE Trans. Signal Process.*, vol. 65, no. 4, pp. 933–946, Feb. 2017.
- [12] Y. Zeng, J. Chen, J. Xu, D. Wu, X. Xu, S. Jin, X. Gao, D. Gesbert, S. Cui, and R. Zhang, "A tutorial on environment-aware communications via channel knowledge map for 6G," *IEEE Commun. Surv. Tuts.*, vol. 26, no. 3, pp. 1478–1519, 3rd Quart. 2024.
- [13] Q. Wu, S. Zhang, B. Zheng, C. You, and R. Zhang, "Intelligent reflecting surface-aided wireless communications: A tutorial," *IEEE Trans. Commun.*, vol. 69, no. 5, pp. 3313–3351, May 2021.
- [14] M. Di Renzo, A. Zappone, M. Debbah, M.-S. Alouini, C. Yuen, J. De Rosny, and S. Tretyakov, "Smart radio environments empowered by reconfigurable intelligent surfaces: How it works, state of research, and the road ahead," *IEEE J. Sel. Areas Commun.*, vol. 38, no. 11, pp. 2450–2525, Nov. 2020.
- [15] H. Lu, Y. Zeng, S. Jin, and R. Zhang, "Aerial intelligent reflecting surface: Joint placement and passive beamforming design with 3D beam flattening," *IEEE Trans. Wireless Commun.*, vol. 20, no. 7, pp. 4128–4143, Jul. 2021.
- [16] W. Tang, M. Z. Chen, X. Chen, J. Y. Dai, Y. Han, M. Di Renzo, Y. Zeng, S. Jin, Q. Cheng, and T. J. Cui, "Wireless communications with reconfigurable intelligent surface: Path loss modeling and experimental measurement," *IEEE Trans. Wireless Commun.*, vol. 20, no. 1, pp. 421–439, 2020.
- [17] J. Ryerson, "Passive satellite communication," *Proc. IRE*, vol. 48, no. 4, pp. 613–619, Apr. 1960.
- [18] C. C. Cutler, "Passive repeaters for satellite communication systems," Feb. 1965, U.S. Patent 3 169 245.
- [19] Y. Rahmat-Samii and R. Haupt, "Reflector antenna developments: a perspective on the past, present and future," *IEEE Antennas Propag. Mag.*, vol. 57, no. 2, pp. 85–95, Apr. 2015.
- [20] C. A. Balanis, *Antenna theory: Analysis and design*. Hoboken, NJ, USA: Wiley, 2016.
- [21] Y. Huang, N. Yi, and X. Zhu, "Investigation of using passive repeaters for indoor radio coverage improvement," in *Proc. IEEE Int. Symp. Antennas Propag.*, vol. 2, Jun. 2004, pp. 1623–1626.
- [22] J. Chan, C. Zheng, and X. Zhou, "3D printing your wireless coverage," in *Proc. ACM Int. Workshop Hot Topics Wireless (HotWireless)*, Sep. 2015, pp. 1–5.
- [23] S. Han and K. G. Shin, "Enhancing wireless performance using reflectors," in *Proc. IEEE INFOCOM-IEEE Conf. Comput. Commun.*, May 2017, pp. 1–9.
- [24] W. Khawaja, O. Ozdemir, Y. Yapici, F. Erden, and I. Guvenc, "Coverage enhancement for NLOS mmWave links using passive reflectors," *IEEE Open J. Commun. Soc.*, vol. 1, pp. 263–281, Jan. 2020.
- [25] S. Häger, K. Heimann, S. Böcker, and C. Wietfeld, "Holistic enlightening of blackspots with passive tailorable reflecting surfaces for efficient urban mmWave networks," *IEEE Access*, vol. 11, pp. 39 318–39 332, Apr. 2023.
- [26] C. K. Anjinappa, F. Erden, and I. Güvenc, "Base station and passive reflectors placement for urban mmWave networks," *IEEE Trans. Veh. Technol.*, vol. 70, no. 4, pp. 3525–3539, Apr. 2021.
- [27] S. Singh, H. Tran, and T. Le, "Stabilizing terahertz MIMO channel capacity with controlled diffuse reflections," in *Proc. IEEE Int. Conf. Commun. (ICC)*, May 2023, pp. 5824–5830.
- [28] Z. Yu, C. Feng, Y. Zeng, T. Li, and S. Jin, "Wireless communication using metal reflectors: Reflection modelling and experimental verification," in *Proc. IEEE Int. Conf. Commun. (ICC)*, May 2023, pp. 4701–4706.
- [29] J. L. D. L. T. Barreiro and F. L. E. Azipiroz, "Passive reflector for a mobile communication device," Aug. 2006, U.S. Patent 7 084 819.
- [30] Ö. Özdoğan, E. Björnson, and E. G. Larsson, "Intelligent reflecting surfaces: Physics, propagation, and pathloss modeling," *IEEE Wireless Commun. Lett.*, vol. 9, no. 5, pp. 581–585, May 2020.
- [31] L. Zhu, W. Ma, and R. Zhang, "Movable antennas for wireless communication: Opportunities and challenges," *IEEE Commun. Mag.*, vol. 62, no. 6, pp. 114–120, Jun. 2024.
- [32] —, "Modeling and performance analysis for movable antenna enabled wireless communications," *IEEE Trans. Wireless Commun.*, vol. 23, no. 6, pp. 6234–6250, Jun. 2024.
- [33] W. Ma, L. Zhu, and R. Zhang, "MIMO capacity characterization for movable antenna systems," *IEEE Trans. Wireless Commun.*, vol. 23, no. 4, pp. 3392–3407, Apr. 2024.
- [34] X. Shao, Q. Jiang, and R. Zhang, "6D movable antenna based on user distribution: Modeling and optimization," *IEEE Trans. Wireless Commun.*, 2024, doi: 10.1109/TWC.2024.3492195.
- [35] X. Shao, R. Zhang, Q. Jiang, and R. Schober, "6D movable antenna enhanced wireless network via discrete position and rotation optimization," *IEEE J. Sel. Areas Commun.*, 2024.
- [36] X. Shao and R. Zhang, "6DMA enhanced wireless network with flexible antenna position and rotation: Opportunities and challenges," *IEEE Commun. Mag.*, 2024.
- [37] B. Ning, S. Yang, Y. Wu, P. Wang, W. Mei, C. Yuen, and E. Björnson, "Movable antenna-enhanced wireless communications: General architectures and implementation methods," *arXiv preprint arXiv:2407.15448*, 2024.
- [38] J. Diebel *et al.*, "Representing attitude: Euler angles, unit quaternions, and rotation vectors," *Matrix*, vol. 58, no. 15-16, pp. 1–35, Oct. 2006.